An eddifying Stommel model: Fast eddy effects in a two-box ocean

William Barham and Ian Grooms*

Department of Applied Mathematics, University of Colorado, Boulder, CO 80309

(*March 27, 2018*)

A system of stochastic differential equations is formulated describing the heat and salt content of a two-box ocean. Variability in the heat and salt content and in the thermohaline circulation between the boxes is driven by fast Gaussian atmospheric forcing and by ocean-intrinsic eddy-driven variability. The eddy forcing of the slow dynamics takes the form of a colored, non-Gaussian noise. The qualitative effects of this non-Gaussianity are investigated by comparing to two approximate models: one that includes only the mean eddy effects (the 'averaged model'), and one that includes an additional Gaussian white-noise approximation of the eddy effects (the 'Gaussian model'). Both of these approximate models are derived using the methods of fast averaging and homogenization.

In the parameter regime where the dynamics has a single stable equilibrium the averaged model has too little variability. The Gaussian model has accurate second-order statistics, but incorrect skew and rare-event probabilities. In the parameter regime where the dynamics has two stable equilibria the eddy noise is much smaller than the atmospheric noise. The averaged, Gaussian, and non-Gaussian models all have similar stationary distributions, but the jump rates between equilibria are too small for the averaged and Gaussian models.

Keywords: Slow-fast systems; averaging; homogenization; stochastic differential equations; ocean modeling

1. Introduction

H. Stommel (1961) developed a conceptual model of the global ocean thermohaline circulation that consists of a system of ordinary differential equations modeling the heat and salt content of two containers ('boxes'). One box models the equatorial ocean, and the other models the extra-tropical ocean. The boxes exchange heat and freshwater with each other and with the atmosphere. The rate of flow between the boxes is proportional to the density difference between the boxes, and a major result of Stommel's investigation was that in some parameter regimes the system exhibits two equilibria: one analogous to the current climate, with dense cold water sinking at high latitudes, and one corresponding to a very different regime with dense salty water sinking in the equatorial ocean. In general, the goal of studies using extremely simplified models like Stommel's is to observe and understand qualitative features that might inform and guide subsequent studies using more complete and more complex models. The qualitative predictions of Stommel's model have since been verified using more complete ocean models, e.g. Rahmstorf (1995) and Deshayes *et al.* (2013).

The present investigation develops a model closely related to Stommel's where the slow, density-driven exchange of heat and salt between the boxes is augmented by fast, non-Gaussian stochastic processes representing eddy-driven heat and salt transport. Eddies smaller than the grid scale of comprehensive numerical ocean (and atmosphere) models can have significant impacts on the global circulation, and modeling the impacts of these unresolved eddies is a topic of continuing research; Berner *et al.* (2017) and Leutbecher *et al.* (2017) contain reviews

---

*Corresponding author. Email: ian.grooms@colorado.edu

of stochastic models of eddy effects from an operational modeling perspective.

The second author recently proposed a non-Gaussian model of the heat and salt transport associated with unresolved ocean eddies (Grooms 2016). In this model, the eddy velocity and density fields (the latter linearly related to temperature and salinity) are modeled as centered Gaussian random fields, and the transports are modeled as the product of eddy velocity and density. The product of centered, jointly Gaussian random variables has a distinctive, non-Gaussian probability density with a logarithmic singularity at the origin and skewed, algebraically-modulated exponential decay in the tails. This non-Gaussian model is significantly different from recent Gaussian stochastic models of eddy transport, e.g. Andrejczuk *et al.* (2016), Williams *et al.* (2016) and Juricke *et al.* (2017). The present investigation is motivated by the desire to observe the qualitative effects of the kind of non-Gaussian transport from Grooms (2016) in an extremely simple model, in particular by comparison to Gaussian stochastic models, with the expectation of informing future investigations using more complex models.

A very wide range of stochastic parameterizations for ocean models of various resolutions with various kinds of Gaussian and non-Gaussian noise are currently under development, e.g. Porta Mana and Zanna (2014), Zanna *et al.* (2017), M´emin (2014), Resseguier *et al.* (2017), Grooms *et al.* (2015), Holm (2015), Cotter *et al.* (2017), Cooper (2017), and Brankart *et al.* (2015), in addition to those cited previously and many more too numerous to cite. The present study is intended to investigate the qualitative differences between a stochastic parameterization with a specific kind of non-Gaussian noise from Grooms (2016), a deterministic parameterization, and a Gaussian stochastic parameterization in a highly idealized model. As noted by Held (2005), the relationship of highly idealized models like the Stommel model to more complex and comprehensive climate models is analogous to the relationship between the fruit fly *Drosphila melanogaster* and *Homo sapiens*. Very few specific conclusions about the latter can be drawn from the former, but the study of the former is nevertheless invaluable in developing a broader understanding of generic features of biology.

Several authors have developed stochastic versions of Stommel's model to investigate the slow response of the ocean thermohaline circulation to fast atmospheric forcing, e.g. Cessi (1994), V´elez-Belchı *et al.* (2001), Monahan (2002), Monahan *et al.* (2002) and Monahan and Culina (2011). In these stochastic Stommel models the atmospheric heat and freshwater fluxes in Stommel's model are replaced by Gaussian stochastic noise terms, resulting in a system of stochastic differential equations (SDEs). The model developed here attempts to understand a qualitatively different physical process: fast eddy transport. Since the eddies are typically faster than the global thermohaline circulation, the new model has the form of a slow-fast system, where eddy variables evolve on a fast time scale and converge towards a jointly Gaussian distribution conditioned on the slow variables. The slow variables (the heat and salt difference between the boxes) are impacted by quadratic products of fast variables modeling the fast eddy transport. The formal theory of fast averaging (Papanicolaou and Kohler 1974, Pavliotis and Stuart 2008, Freidlin and Wentzell 2012), is used to generate approximate slow systems for comparison: one with a drift correction and one with both drift and diffusion corrections derived from the eddy dynamics. These approximate systems qualitatively represent more complete ocean models with, respectively, deterministic and Gaussian stochastic models of the eddy transport.

A new stochastic Stommel model including fast eddy transport is developed in *§2*. The two approximate models of the slow system are derived in *§3*. The numerical methods and experimental configuration are described in *§4* and the results of these simulations are described in *§5*. A slightly different model with two stable equilibria is formulated and simulated in *§6*. The results and their implications are discussed in *§7*.

70 **2.   Formulating a Slow-Fast Two-Box Stochastic Ocean Model**

71 This section recalls the derivation of the original Stommel model by considering the conser-
72 vation of heat and salt in an ocean basin divided into two subdomains that exchange heat
73 and salt with each other, and are forced by heat and freshwater fluxes from the atmosphere.
74 The novel component of the derivation is to add stochastic eddy-driven fluxes between
75 the subdomains. Consistent with the goal of this investigation the eddy-driven exchange is
76 constructed as the product of centered Gaussian eddy velocity, heat, and salt anomalies; the
77 flux distribution is thus qualitatively similar to the flux distributions recently observed by
78 Grooms (2016). Naturally, other eddy flux models are possible; a Gaussian white noise model
79 is, for example, derived in §3.
80
81   Consider a domain $[0, L_x] \times [0, L_y] \times [0, H]$ representing an ocean basin, and let this domain
82 be partitioned into two subdomains $[0, L_x] \times [0, \ell] \times [0, H]$ and $[0, L_x] \times [\ell, L_y] \times [0, H]$ with
83 volumes $V_1 = L_x \ell H$ and $V_2 = L_x(L_y - \ell)H$. The first box (index 1) will represent the equatorial
84 side of the ocean basin, and the second (index 2) will represent the poleward side. The domain
85 is filled with a fluid whose density is related to its temperature and salinity via

$$\rho = \rho_0[1 + \alpha_S(S - S_0) - \alpha_T(T - T_0)]$$

86 where $\rho_0 = 1029$ kg/m^3 is a constant reference density, $T_0 = 5$ C and $S_0 = 35$ psu are a
87 constant reference temperature and salinity (psu are practical salinity units; for the present
88 purposes it is reasonable to use the simplification 1 psu = 1 g/kg), $\alpha_S = 7.5 \times 10^{-4}$ psu^{-1}
89 and $\alpha_T = 1.7 \times 10^{-4}$ C^{-1} are coefficients of haline and thermal expansion. The conservation
90 equations for heat are in the form of a system of two differential equations

$$\frac{\mathrm{d}T_1}{\mathrm{d}t} = -\frac{1}{\tau_T}(T_1 - T_1^*) - \frac{F_T}{\rho_0 c_p V_1}, \quad \frac{\mathrm{d}T_2}{\mathrm{d}t} = -\frac{1}{\tau_T}(T_2 - T_2^*) + \frac{F_T}{\rho_0 c_p V_2}$$

91 where T_1 and T_2 are the mean temperature in each box, τ_T is the timescale of relaxation
92 towards an externally-specified atmospheric temperature T^*, $c_p = 4000$ J/kg is the heat
93 capacity of seawater (e.g. $\rho_0 c_p V_1 T_1$ is the heat content of the equatorial box), and F_T is the
94 heat flux from the equatorial box to the poleward box. The total heat content ($c_p(V_1 T_1 + V_2 T_2)$)
95 thus depends only on the external forcing.
96   Similarly, the conservation equations for salt are

$$\frac{\mathrm{d}S_1}{\mathrm{d}t} = \frac{1}{2}F(t) - F_S, \quad \frac{\mathrm{d}S_2}{\mathrm{d}t} = -\frac{1}{2}F(t) + F_S$$

97 where $F(t)/2$ is the external freshwater forcing in the equatorial box (e.g. rain, runoff, evap-
98 oration) and F_S is the salt flux from the equatorial box to the poleward box. The external
99 freshwater forcing is assumed not to change the net salt content, so that $S_1 + S_2$ remains
100 constant in time.
101   Following Stommel (1961), the heat and salt fluxes between the boxes are assumed to
102 depend only on the temperature and salinity differences between the boxes. As a result, the
103 temperature and salinity differences between the boxes decouple from the net heat and salt
104 content. Defining $\Delta T = T_1 - T_2$ and $\Delta S = S_1 - S_2$,

$$\frac{\mathrm{d}\Delta T}{\mathrm{d}t} = -\frac{1}{\tau_T}(\Delta T - \Delta T^*) - \left(\frac{1}{\rho_0 c_p V_1} + \frac{1}{\rho_0 c_p V_2}\right)F_T$$

105

$$\frac{\mathrm{d}\Delta S}{\mathrm{d}t} = F(t) - 2F_S.$$

106 Similar to Cessi (1994) and V´elez-Belchı *et al.* (2001), the atmospheric temperature difference
107 ΔT^* and external freshwater forcing $F(t)$ are here modeled as constant mean terms plus

108 Gaussian white noise, leading to

$$\mathrm{d}\Delta T = \left[-\frac{1}{\tau_T}(\Delta T - \overline{\Delta T^*}) - \left(\frac{1}{\rho_0 c_p V_1} + \frac{1}{\rho_0 c_p V_2} \right) F_T \right] \mathrm{d}t + \frac{\sigma_{\Delta T}}{\sqrt{\overline{\tau_T}}}\mathrm{d}W_{\Delta T}$$

109

$$\mathrm{d}\Delta S = \left[\overline{F} - 2F_S \right] \mathrm{d}t + \frac{\sigma_{\Delta S}}{\sqrt{\overline{\tau_d}}}\mathrm{d}W_{\Delta S}.$$

110 The amplitude of the atmospheric heat flux noise forcing is here scaled by $\sqrt{\tau_T}$ so that it
111 generates temperature perturbations of amplitude $\sigma_{\Delta T}$ over a time period of length τ_T; the
112 atmospheric freshwater flux noise is similarly scaled to generate perturbations of amplitude
113 $\sigma_{\Delta S}$ over a diffusive time τ_d, defined below.
114   In Stommel's original model the fluxes between the boxes consist of diffusive fluxes pro-
115 portional to the temperature and salinity differences, and advective fluxes associated with
116 the large-scale ocean circulation whose rate is proportional to the magnitude of the density
117 difference between the boxes

$$\left(\frac{1}{\rho_0 c_p V_1} + \frac{1}{\rho_0 c_p V_2} \right) F_T = \left[\frac{1}{\tau_d} + \frac{1}{\tau_a \rho_0 \alpha_T \overline{\Delta T^*}}|\Delta\rho| \right] \Delta T$$

118

$$2F_S = \left[\frac{1}{\tau_d} + \frac{1}{\tau_a \rho_0 \alpha_T \overline{\Delta T^*}}|\Delta\rho| \right] \Delta S$$

119 where τ_d is the time scale of diffusive transport, τ_a is the time scale of advective transport,
120 and

$$\Delta\rho = \rho_0[\alpha_S \Delta S - \alpha_T \Delta T]$$

121 is the density difference between the boxes. Cessi (1994) used a smoother formulation, which
122 does not qualitatively change the results

$$\left(\frac{1}{\rho_0 c_p V_1} + \frac{1}{\rho_0 c_p V_2} \right) F_T = \left[\frac{1}{\tau_d} + \frac{1}{\tau_a (\rho_0 \alpha_T \overline{\Delta T^*})^2}\Delta\rho^2 \right] \Delta T$$

123

$$2F_S = \left[\frac{1}{\tau_d} + \frac{1}{\tau_a (\rho_0 \alpha_T \overline{\Delta T^*})^2}\Delta\rho^2 \right] \Delta S.$$

124   The novel contribution to the model made here consists of the addition of fast variables
125 crudely representing eddy velocity v_e, temperature T_e and salinity S_e anomalies at the in-
126 terface between the boxes. The eddy-induced fluxes between the boxes will be modeled as an
127 addition to the slow diffusive and advective fluxes

$$\left(\frac{1}{\rho_0 c_p V_1} + \frac{1}{\rho_0 c_p V_2} \right) F_T = \left[\frac{1}{\tau_d} + \frac{1}{\tau_a (\rho_0 \alpha_T \Delta T^*)^2}\Delta\rho^2 \right] \Delta T + \left(\frac{1}{\ell} + \frac{1}{L_y - \ell} \right) v_e T_e$$

128

$$2F_S = \left[\frac{1}{\tau_d} + \frac{1}{\tau_a (\rho_0 \alpha_T \Delta T^*)^2}\Delta\rho^2 \right] \Delta S + \left(\frac{1}{\ell} + \frac{1}{L_y - \ell} \right) v_e S_e.$$

129 The prefactors of $\ell^{-1} + (L_y - \ell)^{-1}$ account for the fact that the boxes need not have equal
130 volume, and that total heat and salt need to be conserved. For simplicity, only $\ell = L_y/2$ is
131 considered from here on.
132   In general the flux between the boxes should be described by $\int_0^{R_I} \int_0^{R_H} vT \, \mathrm{d}z\mathrm{d}x$ where v and T
133 are evaluated at $y = \ell$, $y \neq 2L$. Our formulation amounts to a severe simplification that ignores
134 the spatial structure of the eddy velocity and temperature perturbations between the boxes,
135 and considers them only as zero-mean jointly-Gaussian variables. This level of simplification is
136 consistent with the simplification of the ocean to two well-mixed boxes in the original Stommel

137 model,and is guided by the desire to investigate the qualitative effects of Gaussian-product
138 noise, since eddy noise with this structure was recently observed by Grooms (2016).
139   The fast eddy velocity will be modeled as an Ornstein-Uhlenbeck process

$$dv_e = -\frac{1}{\tau_e}v_e dt + \sqrt{\frac{2}{\tau_e}}\sigma_v dW_v$$

140 where τ_e is the eddy time scale and σ_v is the eddy velocity scale,chosen to be 15 days and
141 10 cm/s, respectively (Stammer 1997). The eddy velocity can here be thought of as being set
142 by wind-driven processes independent of the density difference between the boxes.This is a
143 simplification of the more complex reality where eddy kinetic energy and time scale depend
144 also on the large-scale density gradient. The following model of the eddy dynamics is perhaps
145 more qualitatively appropriate

$$dv_e = -\frac{v_e}{\tau_e}dt + \sqrt{\frac{2(1+\mu\Delta\hat{\rho})}{\tau_e}}dW_v$$

146 where $\mu > 0$ is a parameter representing the sensitivity of the eddy variance to the large-scale
147 density gradient. This model is not pursued further here, in part because of the difficulties in
148 guaranteeing its ergodicity and in finding a robust numerical method for its solution.
149   The eddy temperature and salinity anomalies will be modeled as resulting from eddy trans-
150 port across the large-scale gradients

$$\frac{dT_e}{dt} = -\frac{T_e}{\tau_e} - v_e\frac{2\Delta T}{L_y},$$

151

$$\frac{dS_e}{dt} = -\frac{S_e}{\tau_e} - v_e\frac{2\Delta S}{L_y}.$$

152 The relaxation towards zero on a time scale of τ_e qualitatively represents the full range of
153 dissipative processes acting on temperature and salinity anomalies:cascade towards small
154 scales and eventual diffusion, and atmospheric damping of thermal anomalies, etc. The time
155 scale τ_e should not be associated with any particular physical process, but instead guarantees
156 decorrelation of eddy anomalies on the time scale τ_e. Note that the lack of white noise forcing
157 in the equations for T_e and S_e implies that the amplitude of the eddy terms is governed by
158 σ_v; if $\sigma_v = 0$ then the eddy terms disappear, leaving the usual Stommel model.
159   The governing equations are nondimensionalized using the diffusive time scale for t, the ex-
160 ternal constant atmospheric temperature difference $\overline{\Delta T} \approx 20°C$ for large-scale temperature,
161 and the convenient salinity scale $\alpha_T\overline{\Delta T}/\alpha_S \approx 4.5$ psu for large-scale salinity. The mean atmo-
162 spheric forcing $\overline{g}$ is assumed to be 4.5 psu per diffusion time so that its nondimensional value
163 is 1, following Cessi (1994) and V´elez-Belchı *et al.* (2001). The eddy velocity v_e is nondimen-
164 sionalized using the eddy velocity scale σ_v. It will be convenient to scale the eddy temperature
165 and salinity variables differently, specifically T_e will have dimensions $\overline{\Delta T}\Delta L_y/(\sigma_v\tau_d)$ and S_e
166 will have dimensions $\alpha_T\overline{\Delta T} *L_y/(\alpha_S\sigma_v\tau_d)$. The reason for this unexpected scaling will be com-
167 mented on shortly.
168   Following traditional notation, the nondimensional temperature difference will be denoted x
169 and the nondimensional salt difference will be denoted y. The nondimensional eddy variables
170 will drop their subscripts e so that, e.g., the nondimensional eddy velocity is simply v. Risking
171 confusion,the nondimensional time will still be denoted t.The complete nondimensional
172 system is therefore

W. Barham and I. Grooms

$$\mathrm{d}x = -\frac{1}{T}(x-1) - [1 + P_a(x-y)^2]x + 4vT\,\mathrm{d}t + \sqrt{\frac{1}{T}}\sigma_x\mathrm{d}W_x \tag{1a}$$

$$\mathrm{d}y = 1 - [1 + P_a(x-y)^2]y + 4vS\,\mathrm{d}t + \sigma_y\mathrm{d}W_y \tag{1b}$$

$$\mathrm{d}v = -\frac{v}{}\,\mathrm{d}t + \sqrt{2}\,\mathrm{d}W_v \tag{1c}$$

$$\mathrm{d}T = -\frac{1}{}\,T + 2P^2vx\ \mathrm{d}t \tag{1d}$$

$$\mathrm{d}S = -\frac{1}{}\,S + 2P^2vy\ \mathrm{d}t \tag{1e}$$

173 where

$$T = \frac{\tau_T}{\tau_d}, \quad = \frac{\tau_e}{\tau_d}, \ P_a = \frac{\tau_d}{\tau_a}, \ P_e = \frac{\sigma_v\tau_d}{L_y}, \ P = \sqrt{P_e}.$$

174 P_a and P_e are Péclet numbers comparing the time scales of large scale advective transport
175 and fast eddy transport to the time scale of diffusion, respectively. The nondimensional noise
176 amplitudes are $\sigma_x = \sigma_{\Delta T}/\overline{\Delta T}^*$ and $\sigma_y = \alpha_S\sigma_{\Delta S}/(\alpha_T\overline{\Delta T}^*)$.
177   The following parameter estimates are drawn from Cessi (1994) and Vélez-Belchí *et al.*
178 (2001), and are consistent with the more recent observational analysis of Schmitt (2008).
179 The diffusive time scale τ_d is approximately 220 years, and the time scale of large scale
180 advection τ_a is approximately 35 years. Cessi (1994) estimates τ_e to be 25 days, but Vélez-
181 Belchí *et al.* (2001) argue convincingly that large-scale temperature anomalies are damped
182 on a slower time scale of approximately 220 days. Vélez-Belchí *et al.* (2001) used salinity
183 noise whose nondimensional amplitude is $\sigma_y = 0.15$, and assuming that fast atmospheric
184 temperature fluctuations lead to perturbations on the order of 0.07 C implies nondimensional
185 thermal noise has amplitude $\sigma_x = 0.005$. Finally, using a length scale appropriate to the
186 global oceans $L_y \approx 8{,}250$ km leads to the following set of parameters which are adopted for
187 the remainder of the investigation

$$T = \frac{1}{400}, \quad = \frac{1}{5000}, \ P_a = 6, \ P_e = 80, \ \sigma_x = 0.005, \sigma_y = 0.15. \tag{2}$$

188 The reason for scaling S and T differently from ΔS and ΔT should now be clear: P_e is the $2P^2$
189 same order of magnitude as 1, implying that both terms in the evolution equations for S
190 and T are of comparable magnitude.
191   For the parameters (2) the system (1) has three equilibria, two of which are stable. The
192 equilibria all have $v, T, S = 0$, and the stable equilibria occur at $(x, y) \approx (0.989, 0.22)$ and
193 $(x, y) \approx (0.998, 1.00)$. In the absence of eddy dynamics, one would expect small atmospheric
194 noise to lead to jumping between the two stable equilibria of the system; this was the focus
195 of Cessi (1994), Monahan (2002), Monahan *et al.* (2002) and Monahan and Culina (2011).
196   The existence of multiple equilibria is intrinsically tied to the nonlinear terms that model
197 slow advective exchange between the boxes. As the exchange between the boxes becomes
198 dominated by diffusion instead of advection (P_a) one of the stable equilibria disappears
199 in a reverse saddle-node bifurcation leaving a single stable equilibrium.
200
201   Equations (1d) and (1e) lack noise terms, implying that the classical conditions for ergodicity
202 (Khasminskii 2012) do not apply. Conditions for ergodicity of this type of system of SDEs
203 can be found in Mattingly *et al.* (2002). The first condition is that there is an inner-product
204 norm $\|\cdot\|$ such that $\langle u, F(u)\rangle \le \alpha - \beta\|u\|^2$ for some $\alpha, \beta > 0$ where u is a vector containing

the dependent variables and $\boldsymbol{F}(\boldsymbol{u})$ is the drift. It is straightforward to verify that $k|\boldsymbol{u}|^2 = x^2 + y^2 + v^2 + (2/P^2)(T^2 + S^2)$ satisfies this condition. The second condition is that the vectors $\{\boldsymbol{\rho}_i, [[\boldsymbol{F}, \boldsymbol{\rho}_j], \boldsymbol{\rho}_k]\}$ span $\mathbb{R}^5$ where $\boldsymbol{\rho}_i$, $i = 1, 2, 3$ are the columns of the diffusion matrix, which are here proportional to the first three standard basis vectors, and $[\cdot, \cdot]$ is a Lie bracket. Since $[[\boldsymbol{F}, \boldsymbol{\rho}_1], \boldsymbol{\rho}_1]$ and $[[\boldsymbol{F}, \boldsymbol{\rho}_1], \boldsymbol{\rho}_1]$ are proportional to the fourth and fifth standard basis vectors, respectively, the system satisfies the conditions of Mattingly *et al.* (2002) for ergodicity.

3. Two Approximate Slow Models

In this section two systems of SDEs are derived approximating the evolution of the slow variables x and y in (1). The system of SDEs (1) with parameters (2) has three time scales since $\epsilon < \tau \ll 1$: x evolves significantly more quickly than y, yet slower than the eddy variables v, T, and S. Many previous investigations (which lacked the eddy variables) accounted for the scale separation somewhat crudely by setting $x = 1$, and focused on the dynamics of the slowest variable y, e.g. Cessi (1994), Monahan (2002), Monahan *et al.* (2002), and Monahan *et al.* (2008). The analysis of Monahan and Culina (2011) is more careful, employing the same methods used here but for the system without eddy variables and in the limit $\tau \to 0$. This section considers the limit $\epsilon \to 0$ while holding τ fixed.

The two approximate models are derived using standard approximations for slow-fast systems (Papanicolaou and Kohler 1974, Pavliotis and Stuart 2008, Freidlin and Wentzell 2012). The presentation here follows the convenient review found in Bouchet *et al.* (2016); the formulas are derived in a straightforward manner using formal asymptotic methods applied to the backwards Kolmogorov equation for the system (for details, see the appendices of Bouchet *et al.* (2016)).

The first approximation is derived via simple averaging. In the limit $\epsilon \to 0$ the eddy variables are well approximated as solutions to (1c)–(1e) with x and y considered constant. Curiously, although the full system (1) has a smooth invariant measure the system (1c)–(1e) does not: the long-time limiting distribution of v, T, and S is jointly Gaussian with a singular covariance matrix. In light of this, the following noise-augmented system is considered instead

$$dv = -\frac{v}{\epsilon}dt + \sqrt{\frac{2}{\epsilon}}dW_v \tag{3a}$$

$$dT = -\frac{1}{\epsilon}\left(T + 2P^2vx\right)dt + \sqrt{\frac{2}{\epsilon}}\sigma\,dW_T \tag{3b}$$

$$dS = -\frac{1}{\epsilon}\left(S + 2P^2vy\right)dt + \sqrt{\frac{2}{\epsilon}}\sigma\,dW_S \tag{3c}$$

and the limit $\sigma \to 0$ is taken after the fact.

The invariant measure of (3) is Gaussian with zero mean and covariance

$$\begin{bmatrix} 1 & -P^2x & -P^2y \\ -P^2x & 2P^4x^2 + \sigma^2 & 2P^4xy \\ -P^2y & 2P^4xy & 2P^4y^2 + \sigma^2 \end{bmatrix}. \tag{4}$$

The averages of the terms vT and vS in the slow equations with respect to the invariant measure of the fast system are simply $-P^2x$ and $-P^2y$, respectively. It is worth noting that these values are independent of the auxiliary noise amplitude σ. Inserting these into the slow equations leads to the following approximate model

239   **Deterministic Approximation**

$$dx = \left[-\frac{1}{T}(x - 1) - [1 + \hat{a}(x - y)^2]x - 4P^2x\right]dt + \sqrt{\frac{1}{T}}\sigma_x dW_x \qquad (5a)$$

$$dy = \left[1 - [1 + \hat{a}(x - y)^2]y - 4P^2y\right]dt + \sigma_y dW_y. \qquad (5b)$$

240 The model (5) is referred to as the 'deterministic' or 'averaged' approximation since it models
241 the eddy terms vT and vS as deterministic functions of x and y. It is straightforward to
242 verify that this model is ergodic under the classical conditions of Khasminskii (2012).
243
244   As described in Bouchet *et al.* (2016), one can derive equations that approximate the varia-
245 tions of the true solution to (1) around the solution of the approximate model (5). Combining
246 the equations for the variations with the deterministic approximation leads to further cor-
247 rections in both the drift and diffusion of order ν and $\sqrt{\nu}$, respectively. The drift correction
248 is significantly smaller than the leading-order drift. But the leading-order diffusion terms in
249 the x and y equations are of order ≈ 0.1, and corrections of order $\sqrt{\nu}$ may be of comparable
250 magnitude.
251   In order to compute the diffusion corrections, it is convenient to define some notation.
252 Let $\mathbf{Y} = (v, T, S)^T$ denote the solution to the noise-augmented system (3). Define constant
253 matrices

$$\mathbf{M} = -\frac{1}{\tau}\begin{bmatrix} 1 & 0 & 0 \\ 2P^2x & 1 & 0 \\ 2P^2y & 0 & 1 \end{bmatrix}, \quad \mathbf{G} = \sqrt{\frac{2}{\tau}}\begin{bmatrix} 1 & 0 & 0 \\ 0 & \sigma & 0 \\ 0 & 0 & \sigma \end{bmatrix}$$

254 such that the fast system (3) may be written $d\mathbf{Y} = \mathbf{M}\mathbf{Y} + \mathbf{G}d\mathbf{W}$, where $d\mathbf{W}$ is a vector of
255 independent Gaussian white noises. The solution is thus

$$\mathbf{Y}(\tau) = e^{\mathbf{M}\tau}\mathbf{Y}_0 + \int_0^\tau e^{\mathbf{M}(\tau-s)}\mathbf{G}d\mathbf{W}. \qquad (6)$$

256 The deviations of the eddy terms vT and vS from their conditional means are denoted

$$\mathbf{f}(x, y, \mathbf{Y}) = \begin{bmatrix} vT + 4P^2x \\ vS + 4P^2y \end{bmatrix}.$$

257 According to Bouchet *et al.* (2016), the diffusion-corrected model for the slow variables has
258 the form

$$dx = \left[-\frac{1}{T}(x - 1) - [1 + \hat{a}(x - y)^2]x - 4P^2x\right]dt$$

$$+ \sqrt{\nu}\,\bar{a}_{xx}(x, y)d\hat{W}_x + \sqrt{\nu}\,\bar{a}_{xy}(x, y)d\hat{W}_y + \sqrt{\frac{1}{T}}\sigma_x dW_x$$

$$dy = \left[1 - [1 + \hat{a}(x - y)^2]y - 4P^2y\right]dt$$

$$+ \sqrt{\nu}\,\bar{a}_{yx}(x, y)d\hat{W}_x + \sqrt{\nu}\,\bar{a}_{yy}(x, y)d\hat{W}_y + \sigma_y dW_y.$$

259 where the matrix

$$\mathbf{A} = \begin{bmatrix} a_{xx} & a_{xy} \\ a_{yx} & a_{yy} \end{bmatrix}$$

260 is any square root of the following symmetric positive definite matrix

$$\mathbf{C} = \int_0^\infty \mathrm{E}^{\mathbf{Y}_0}\left[\mathrm{E}^{\mathbf{Y}(\tau)}\big[\boldsymbol{f}(x, y, \boldsymbol{Y}(\tau))\big]\boldsymbol{f}^T(x, y, \boldsymbol{Y}_0) + \boldsymbol{f}(x, y, \boldsymbol{Y}_0)\mathrm{E}^{\mathbf{Y}(\tau)}\big[\boldsymbol{f}^T(x, y, \boldsymbol{Y}(\tau))\big]\right]\mathrm{d}\tau.$$

261 The matrix $\mathbf{C}$ is the integral of the time-lagged auto-covariance of $\boldsymbol{f}$ with x and y considered
262 constant. In the above expression, $\mathrm{E}^{\mathbf{Y}(\tau)}$ denotes the expectation on $\boldsymbol{Y}(\tau)$ conditioned on the
263 initial condition $\boldsymbol{Y}_0$; the distribution is Gaussian with mean and covariance implied by (6).
264 $\mathrm{E}^{\mathbf{Y}_0}$ denotes expectation on $\boldsymbol{Y}_0$ whose distribution is the stationary distribution of the fast
265 process, in this case a zero-mean Gaussian with covariance (4). The calculation for the system
266 under consideration here is particularly straightforward since it requires only higher moments
267 of jointly-Gaussian variables. The matrix $\mathbf{C}$ is found to have the form

$$\mathbf{C} = \begin{bmatrix} 16(5\bar{P}^4 x^2 + \sigma^2) & 80\bar{P}^4 xy \\ 80\bar{P}^4 xy & 16(5\bar{P}^4 y^2 + \sigma^2) \end{bmatrix}.$$

268 In this case (unlike the leading-order drift term) the limit $\sigma \to 0$ is singular in the sense that
269 the matrix $\mathbf{C}$ becomes positive semi-definite. Nevertheless, a square root matrix $\mathbf{A}$ exists; in
270 the limit $\sigma \to 0$ it has the form

$$\mathbf{A} = 4\sqrt{5}\bar{P}^2 \begin{bmatrix} x & 0 \\ y & 0 \end{bmatrix}.$$

271 The model for the slow variables with leading-order drift and diffusion corrections (but
272 ignoring the order-ϵ drift correction) is thus
273

Gaussian Stochastic Approximation

$$\mathrm{d}x = \left[\frac{1}{\tau}(1 - x) - [1 + a(\bar{P}x - y)^2]x - 4\bar{P}^2 x\right]\mathrm{d}t + 4\sqrt{5}\bar{P}^2 x\mathrm{d}\hat{W} + \sqrt{\frac{1}{\tau}}\sigma_x\mathrm{d}W_x \qquad (7a)$$

$$\mathrm{d}y = \left[1 - [1 + a(\bar{P}x - y)^2]y - 4\bar{P}^2 y\right]\mathrm{d}t + 4\sqrt{5}\bar{P}^2 y\mathrm{d}\hat{W} + \sigma_y\mathrm{d}W_y. \qquad (7b)$$

275 For $x \approx 1$ the noise amplitude associated with the eddies is ≈ 0.16, which is slightly larger
276 than the 'atmospheric' noise $\sigma/\sqrt{\tau} = 0.1$. The order-ϵ drift corrections have also been
277 calculated, but they are small in comparison with the leading-order terms, and have been left
278 out of the model for simplicity. This system of SDEs is interpreted in the Ito sense; while
279 the drift corrections in slow-fast systems with one slow degree of freedom can be interpreted
280 as a correction from Stratonovich to Ito, this is no longer generally true in systems with
281 multiple slow degrees of freedom (Pavliotis and Stuart 2008; Freidlin and Wentzell 2012).
282 It is straightforward to verify that this model is ergodic under the classical conditions of
283 Khasminskii (2012).
284   It is interesting to note that the Gaussian stochastic model replaces the eddy terms $4vT$
285 and $4vS$ by $-4\bar{P}^2 x(\mathrm{d}t + \sqrt{5}\mathrm{d}\hat{W})$ and $-4\bar{P}^2 y(\mathrm{d}t + \sqrt{5}\mathrm{d}\hat{W})$. This form of subgrid-scale pa-
286 rameterization is qualitatively the same as that proposed in Buizza *et al.* (1999), where it was
287 proposed to multiply a deterministic parameterization (here $4\bar{P}^2 x$) by a stochastic process
288 (here $1 + \sqrt{5}\hat{W}$). This style of stochastic parameterization has been widely used in atmo-
289 spheric models (Berner *et al.* (2017) provides a review), and much has been made of the role
290 of multiplicative noise by, e.g. Sura *et al.* (2005). The above derivation gives an example where
291 this style of *ad hoc* parameterization is rigorously justified, though multiplicative noise with a
292 linear coefficient is certainly not the universal form of eddy-induced noise (see e.g. Monahan
293 and Culina 2011, for a counterexample).

294   Recall that for the parameters (2) the system (1) has only three equilibria, two of which
295 are stable. The equilibria all have $v, T, S = 0$, and the stable equilibria occur at $(x, y) \approx$
296 (0.989, 0.22) and $(x, y) \approx$ (0.998, 1.00). The deterministic and Gaussian stochastic models
297 have the same drift, which has only one equilibrium at $(x, y) \approx$ (0.974, 0.093), as will be
298 verified by the results in §5. The inclusion of nonlinear eddy effects completely changes the
299 regime of the ocean model from a regime of multiple equilibria to a regime with a single stable
300 equilibrium.
301   The averaged drift has a single stable equilibrium for all P greater than approximately
302 0.117; below this value the drift undergoes a saddle-node bifurcation that creates a pair of
303 equilibria near $x = 1$ and $y = 1$. To achieve such small values of P would require reducing the
304 eddy velocity scale from 10 cm/s to 1 cm/s, which is unrealistically small. The approximate
305 models derived in this section show that the mean effect of eddies is linear and diffusive. Since
306 a linear diffusive effect is already present in the equations (the terms $-x$ and $-y$ in (1a) and
307 (1b)), the mean eddy effect could be viewed as a double-counting of eddy-induced diffusive
308 exchange between the boxes. This can be rectified by eliminating the mean diffusion terms,
309 and such a model is formulated and studied in §6. By avoiding a double-counting of diffusive
310 exchange, the model in §6 allows multiple equilibria with small, yet realistic eddy amplitudes.

4.   Numerical Methods

312 Numerical methods are needed to compare the qualitative behavior of the three models (1),
313 (5), and (7) . Many methods are derived based on the assumption that the drift is globally-
314 Lipschitz (Kloeden and Platen 1992), which is not the case here. Several more recent investi-
315 gations have analyzed numerical methods for SDEs whose drift satisfies a one-sided Lipschitz
316 condition (e.g. Higham *et al.* (2002) and Mao and Szpruch (2013)), but none of the models in
317 consideration here satisfy such a condition. A method appropriate to polynomial drifts is de-
318 rived by Lamba *et al.* (2007), but their analysis requires an invertible diffusion matrix, which
319 the model (1) does not have. The Euler-Maruyama method may be appropriate, but is known
320 to behave poorly in problems with polynomial drift (Mattingly *et al.* 2002, Hutzenthaler *et al.*
321 2011). In light of this, the 'backward Euler' (BE) method is used here for all three models.
322 For a general system of SDEs of the form

$$d\boldsymbol{X} = \boldsymbol{b}(\boldsymbol{X})\mathrm{d}t + \boldsymbol{\Sigma}(\boldsymbol{X})\mathrm{d}\boldsymbol{W}$$

323 the BE method takes the following form

$$\boldsymbol{X}_{n+1} - \Delta t \boldsymbol{b}(\boldsymbol{X}_{n+1}) = \boldsymbol{X}_n + \boldsymbol{\Sigma}(\boldsymbol{X}_n)\Delta \boldsymbol{W}_n \qquad (8)$$

324 where Δt is the time step. In every simulation presented here $\Delta t = 2 \times 10^{-6}$, which is
325 significantly smaller than the smallest time scale of the system 2×10^{-4}. Mattingly *et al.*
326 (2002) prove that the method is ergodic (for sufficiently small Δt) and that the invariant
327 measure of the numerical method converges to that of the SDE as $\Delta t \to 0$. Though the
328 analysis of Mattingly *et al.* (2002) focuses on models with additive noise, the BE method is
329 nevertheless applied here to the model (7) with multiplicative noise.
330   For the model (1), a two-step process is used to generate solutions of the nonlinear system
331 of equations (8). First, an asymptotic approximation in the limit $\Delta t \to 0$ is computed that
332 has the form $\boldsymbol{X}_* = \boldsymbol{X}_n + \boldsymbol{\Sigma}(\boldsymbol{X}_n)\Delta \boldsymbol{W}_n + O(\Delta t)$; this approximation is followed by a single
333 Newton step. For the systems (5) and (7), approximate solutions to the nonlinear systems
334 were generated using 10 fixed-point iterations started at $\boldsymbol{X}_n$. Given the small step size, the
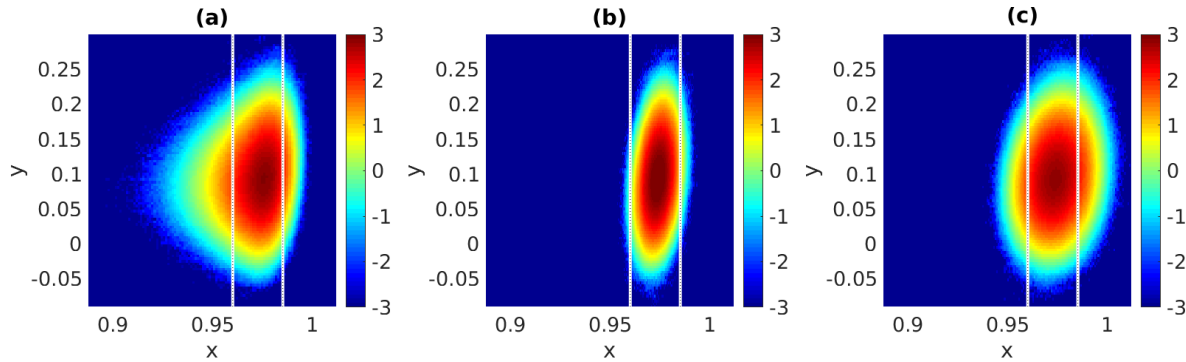335 resulting approximations solve their respective nonlinear systems with high accuracy; the

Figure 1. Base-10 logarithm of the climatological joint probability density functions of *x* and *y* for (a) Full model (1), (b) Deterministic approximation (5), and (c) Gaussian-stochastic approximation (7). The vertical lines are placed at *x* = 0.96 and *x* = 0.985.

336   residuals are typically on the order of 10^{-11}.

337

5.   Results

5.1. *Climatology*

340 A suite of 10,000 independent simulations was run starting from *x, y, v, T, S* = 0 at *t* = 0.
341 Data were saved for the time interval $t \in [4, 10]$, saving every 100th time step for a spacing of
342 2×10^{4}. The mean and covariance appeared to have stabilized by *t* = 4, suggesting that the
343 data in $t \in [4, 10]$ represents the stationary climatological distribution of the system. Recalling
344 that the dimensional time unit is 220 years, this amounts to 1,320 years of data saved approx-
345 imately twice per month. The three models all have the same mean of (*x, y*) ≈ (0.974, 0.094),
346 which is very close to the equilibrium of the deterministic and Gaussian stochastic models at
347 (0.974, 0.093). All three models have the same marginal standard deviation of *y* approximately
348 equal to 0.034. This can be explained by the fact that the amplitude of the eddy noise in the *y*
349 equation is estimated in the Gaussian stochastic model by $\sigma \sqrt{P}/\beta \approx 0.015$ for *y* = 0.093,
350 which is much less than the atmospheric noise with amplitude $\sigma_0 = 0.15$. The parameter
351 values (2) derived from the literature are necessarily imprecise, but the order of magnitude
352 difference between the eddy noise and the atmospheric noise in the *y* equation suggests that
353 the effects of eddy noise (Gaussian or otherwise) on the salinity dynamics of the ocean real
354 may be small in comparison with atmospheric forcing.
355   The climatological distributions of the models differ in other respects. For example, the
356 marginal standard deviation of *x* is 0.0063, 0.0035, and 0.0065 in the full, deterministic, and
357 Gaussian stochastic models, respectively. The eddy noise in the *x* equation is of comparable
358 size to the atmospheric noise, and has a significant impact on the variability; the deterministic
359 model lacks this eddy noise, and has too little variability. The lack of eddy noise in the *x* equa-
360 tion of the deterministic model also leads to an overestimate of the correlation between *x* and
361 *y*: the full and Gaussian stochastic models have correlations 0.15 and 0.14, respectively, while
362 the deterministic model has correlation 0.23. The most-probable values of the distributions
363 are (*x, y*) ≈ (0.976, 0.092) for the full model, (0.974, 0.091) for the deterministic model, and
364 (0.973, 0.093) for the Gaussian stochastic model; the differences in the *y* value are negligible,
365 but the differences in the *x* value are up to half of a standard deviation.
366   Time-lagged correlation functions were computed, for example Corr[$x(t), x(t + \tau)$] = $C(\tau)$
367 (stationarity is assumed). The correlation functions are all very similar across the models (not
368 shown). The correlation functions all decay monotonically to zero, so it is natural to define
369 a decorrelation time by $\int_0^\infty C(\tau)\,d\tau$. The correlation functions for *y* in all three models are

370 very similar, with decorrelation time approximately 22 years. The correlation function for
371 *x* exhibits similar rapid initial decay in all three models. The correlation function for *x* in
372 the deterministic model has a long tail with larger long-lag correlations than the other two
373 models, leading to a decorrelation time of 16 years, which is longer than the decorrelation
374 times of the full model and Gaussian stochastic model, both of which are approximately 1
375 year.
376   A simple binning procedure was used to generate approximations to the climatological prob-
377 ability density function (pdf) for each model; results are shown in Fig. 1, with panels (a)–(c)
378 presenting the full model, deterministic model, and Gaussian stochastic model, respectively.
379 It has already been noted that the three models have the same marginal variance for *y*, and
380 indeed the range of *y* in the three models is quite similar. The deterministic model is clearly
381 under-dispersed with respect to *x*. The climatological distribution of the Gaussian stochastic
382 model has a more-accurate core, but is not skewed in the same way as the full model.
383   It is possible that minor deficiencies near the core of the distribution could be corrected
384 by adding order-ϵ corrections to the drift of the Gaussian stochastic model, but the results
385 of Bouchet *et al.* (2016) indicate that such corrections will not generate correct rare-event
386 probabilities even in the limit $\epsilon \to 0$. To emphasize differences in the rare event probabilities,
387 the probabilities of $x \leq 0.96$ and $x \geq 0.985$ were calculated for the three models (these
388 *x* values are indicated by vertical lines in Fig. 1). The small-event probabilities are 0.039
389 for the full model, less than 10^{-4} for the deterministic model, and 0.022 for the Gaussian
390 stochastic model. The large-event probabilities are 0.016 for the full model, less than 10^{-3} for
391 the deterministic model, and 0.048 for the Gaussian stochastic model. Not surprisingly, the
392 deterministic approximation has too-small event probabilities. The Gaussian-stochastic
393 model is more accurate, but is still incorrect by nearly a factor of 2 for small-event probabilities,
394 and a factor of 3 for large-event probabilities.
395   The system (1) has two stable equilibria, near $(x, y) \approx (1, 1)$ and $(1, 0.22)$. The simulations
396 described above had no trajectories near the stable equilibrium at $(1,1)$; to verify that
397 the system does not remain near the stable equilibrium at $(x, y) \approx (1, 1)$, a set of
398 1,000 simulations of (1) was run with initial condition $(x, y, v, T, S) = (1, 1, 0, 0, 0)$. These
399 simulations were again run for the interval $t \in [0, 10]$, saving the output from $t \in [4, 10]$. The
400 stationary distribution did not display a secondary peak near $(1, 1)$, indicating that the two
401 stable equilibria of the full model are largely irrelevant to the dynamics of the system.
402

5.2. *Rare event forecasting*

404 The previous section examined only the stationary climatological distributions of the three
405 models. Within a climate prediction scenario, short-term behavior is also important. Given
406 that the climatological distributions differ mainly in their rare event probabilities, a separate
407 set of experiments was used to investigate the ability of the models to predict rare events
408 over a shorter time interval. The goal was to test how accurately the approximate models
409 forecast the probability of the unusually large and small *x* values over a range of forecast lead
410 times. Two trajectories of the system (1) were selected out of the 10,000 discussed above: one
411 reaching a value of $x \leq 0.96$ and one reaching a value of $x \geq 0.985$. These trajectories are
412 shown in Fig. 2 panels (a) and (b). Note that the large-*x* trajectory passes the threshold of
413 0.985 approximately half a year before the final time, whereas the small-*x* trajectory crosses
414 the 0.96 threshold only at the last time step. Ensembles of 10,000 independent forecasts for
415 all three models were initialized from the true trajectory for a range of lead times out to 2
416 years. Thus, for each of the three models a 10,000 member ensemble forecast was initialized
417 at $t = -2$ years and run until $t = 0$, and another 10,000 member ensemble forecast was
418 initialized at $t = -1$ year and run until $t = 0$, etc. These ensembles were used to estimate
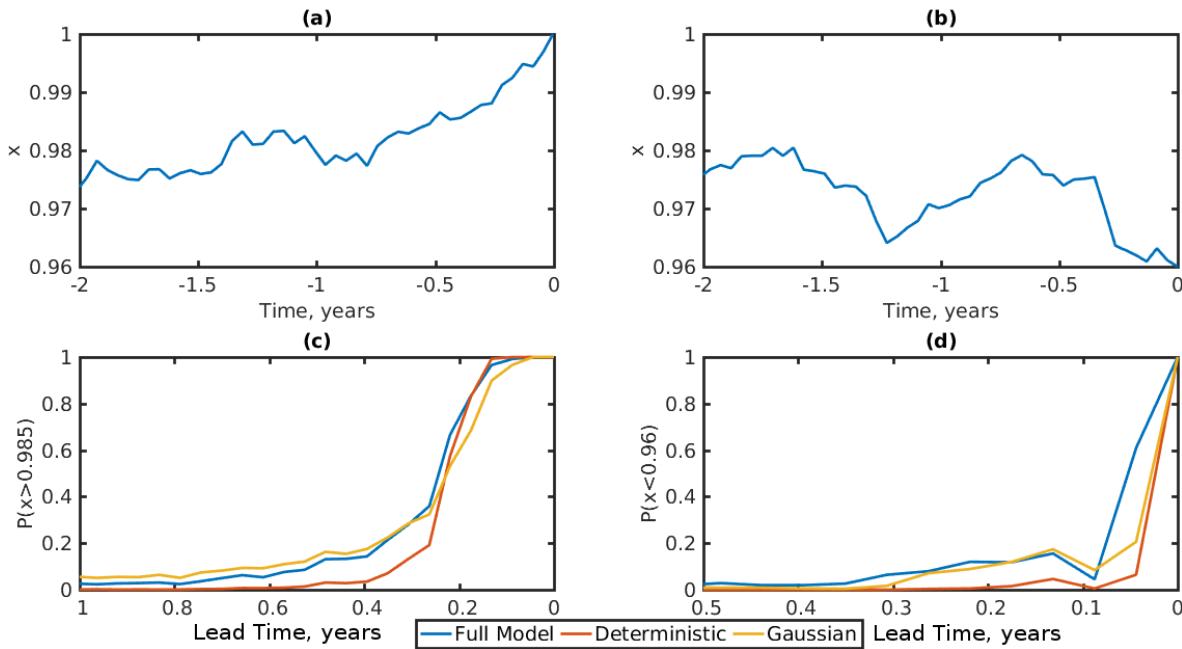
Figure 2. (a) and (b): x trajectories of the full model (1). (c) probability that $x > 0.985$ at $t = 0$, and (d) probability that $x < 0.96$ at $t = 0$ for forecasts initialized from the trajectories in (a) and (b), respectively. Note that the time axes in (c) and (b) are different from each other and from those in (a) and (b).

the probabilities $P\,(x(t = 0) \leq 0.96)$ for the small-event case and $P\,(x(t = 0) \geq 0.985)$ for the large-event case. The probabilities shown in Fig. 2c correspond to the large-x trajectory, and those in Fig. 2d correspond to the small-x trajectory. Since the large-x trajectory crosses the threshold nearly half a year before the final time, all 10,000 of the forecasts initialized at any lead time less than half a year in advance are already above threshold. Nevertheless, the probability at the final time is less than one because many of the trajectories cross the threshold back towards smaller values of x.

In both cases the forecast by the deterministic model is significantly worse that the other two models at all but the shortest lead times. The rare-event probability forecast by the Gaussian stochastic model, in contrast, begins to increase from its climatological value at approximately the same time that the true forecast probability begins to increase, between 0.8 and 0.6 years in advance for the large-x event and around 0.3 years in advance for the small-x event. Although the actual probability assigned by the Gaussian stochastic model at relatively long lead times is incorrect, the fact that it begins to increase at the right time could still be used qualitatively to predict whether the model is getting close to a rare event. Once the probability of a rare event increases past about 20%, the Gaussian stochastic model uniformly under-predicts the correct probability, despite having over-predicted the climatological probability for $x > 0.985$. For example, with a lead time of about 2.5 months the Gaussian stochastic model predicts the large-x event with probability only 53% while the true probability is in fact 67%; with a lead time of half a month the Gaussian stochastic model predicts the small-x event with probability only 21% while the true probability is 61%. Differences in the small-event and large-event predictability for these two cases are probably less related to intrinsic predictability than to the fact that the true trajectory remains above threshold for half a year before the forecast verification time $t = 0$ in the large-event case, while in the small-event case the true trajectory reaches threshold only at $t = 0$.

In summary, the deterministic model is essentially useless for rare-event forecasting, while the Gaussian stochastic model is only qualitatively useful, predicting whether a rare event is more likely but not with a robust uncertainty estimate.

14   *W. Barham and I. Grooms*

447

6.   A model without mean diffusion

As noted at the end of §3, the averaged effect of the eddies is linear and diffusive. Linear diffusive terms are already included in the budgets of heat and salt, with the result that the averaged models have only one stable equilibrium unless the eddies are assumed to be extremely weak, with velocities on the order of 1 cm/s. If one assumes that linear diffusive exchange between the boxes is entirely eddy-driven then one can drop the mean diffusion terms from the governing equations of the full model, i.e. equations (1a) and (1b) are changed to

$$dx = \left[-\frac{1}{T}(x-1) - P_a(x-y)^2 x + 4vT \right] dt + \sqrt{\frac{1}{T}} \sigma_x dW_x \qquad (9)$$

and

$$dy = \left[1 - P_a(x-y)^2 y + 4vS \right] dt + \sigma_y dW_y \qquad (10)$$

respectively. The eddy reductions proceed as before, so that the $-x$ and $-y$ terms are similarly dropped from the deterministic (5) and Gaussian (7) models. The resulting model is much more amenable to multiple equilibria. For P greater than about 0.514 there is a single stable equilibrium with $x \approx 1$ and $y \approx 0.25$. Below this value of P the system undergoes a saddle-node bifurcation that creates a pair of equilibria near $(x, y) = (1, 1)$; the saddle then moves down towards the original equilibrium, which it joins in a reverse saddle-node bifurcation at P approximately 0.301, below which there remains only a single equilibrium. We investigate the system at a value of $P = 9/32$, i.e. $P \approx 0.45$, where there are three equilibria: a stable one at $(.99, .24)$, a saddle at $(1.00, .65)$, and another stable one at $(1.00, 1.11)$.

6.1. *Ergodicity*

Recall that there are two conditions for ergodicity of hypoelliptic SDEs in Mattingly *et al.* (2002). The first condition is that there is an inner-product norm $\|\cdot\|$ such that $\langle \mathbf{u}, \mathbf{F}(\mathbf{u}) \rangle \leq \alpha - \beta \|\mathbf{u}\|^2$ for some $\alpha, \beta > 0$ where $\mathbf{u}$ is a vector containing the dependent variables and $\mathbf{F}(\mathbf{u})$ is the drift. The second condition is that the vectors $\{\boldsymbol{\rho}_i, [\mathbf{F}, \boldsymbol{\rho}_i], [\boldsymbol{\rho}_j, [\mathbf{F}, \boldsymbol{\rho}_i]]\}$ span $\mathbb{R}^5$ where $\boldsymbol{\rho}_i =$ 1, 2, 3 are the columns of the diffusion matrix, and $[\cdot, \cdot]$ is a Lie bracket. It is straightforward to verify that the second condition is met in this model in the same way that it is met in the original model (1).

The first condition is more difficult. We will use the inner product $\langle \mathbf{u}, \mathbf{v} \rangle = u_1 v_1 + u_2 v_2 + u_3 v_3 + (2/P^2)(u_4 v_4 + u_5 v_5)$, so we must show that there are $\alpha, \beta > 0$ such that

$$\langle \mathbf{u}, \mathbf{F}(\mathbf{u}) \rangle - \alpha + \beta \|\mathbf{u}\|^2 \leq 0$$

i.e.

$$-\alpha + y - x(x-1)/T - P_a(x-y)^2(x^2+y^2) - v^2 - (2/P^2)(T^2+S^2)$$
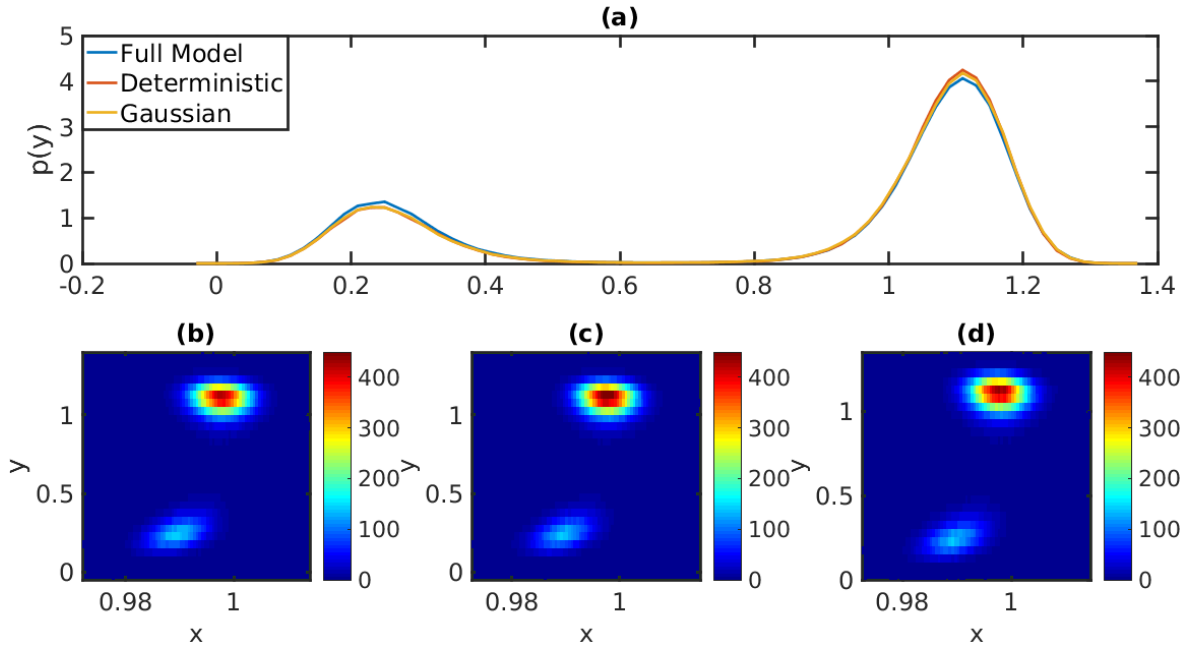$$+ \beta(x^2+y^2+v^2+(2/P^2)(T^2+S^2)) \leq 0.$$

Figure 3. (a) Climatological marginal probability density functions $p(y)$ for the three models without mean diffusion. Climatological joint probability density functions $p(x, y)$ for (b) Full model, (c) Deterministic approximation and (d) Gaussian-stochastic approximation.

477 The terms involving the eddy variables (v, T, and S) will clearly pose no problem provided
478 that $\beta < \tau^{-1}$. It therefore remains to see whether one can choose α, β such that

$$-\alpha + y - x(x - 1)/\tau - P_a(x - y)^2(x^2 + y^2) + \beta(x^2 + y^2) \leq 0.$$

479 Consider the behavior along a line through the origin in the (x, y) plane: along any line except
480 $y = x$ the function is a quartic polynomial that can be made negative by choosing α sufficiently
481 large. Along the line $y = x$ the condition reduces to

$$-\alpha + x - x(x - 1)/\tau + 2\beta x^2 \leq 0.$$

482 As long as $\beta < 1/(2\tau)$ it will be possible to choose α sufficiently large that this condition is
483 met. The model without mean diffusion terms is therefore still ergodic. Ergodicity is important
484 because it implies that there is a single climatological distribution independent of the initial
485 condition; the conditions of Mattingly *et al.* (2002) further guarantee that the distribution
486 collapses exponentially quickly towards the climatological distribution.

487 ### 6.2. *Numerical experiments*

488 Ensemble simulations for the three models without mean diffusion were run with 1000 ensem-
489 ble members each; all parameters are the same as in §5 except $P_e = 32$. The deterministic and
490 Gaussian approximate models were initialized with $x = 1$, $y = 0.6$, while the full model was
491 initialized with $x = 1$, $y = 0.65$, and $v, T, S = 0$. After a burn-in of 4 nondimensional time
492 units, the simulations were run for 500 more time units, i.e. about 110,000 years. Although the
493 models are geometrically ergodic, with distributions collapsing exponentially quickly towards
494 the invariant distribution, this was not enough time for the approximate models to reach the
495 invariant distribution. These models were then extended for a further 500 time units, during
496 which time their distributions converged. The full model was initialized closer to the saddle
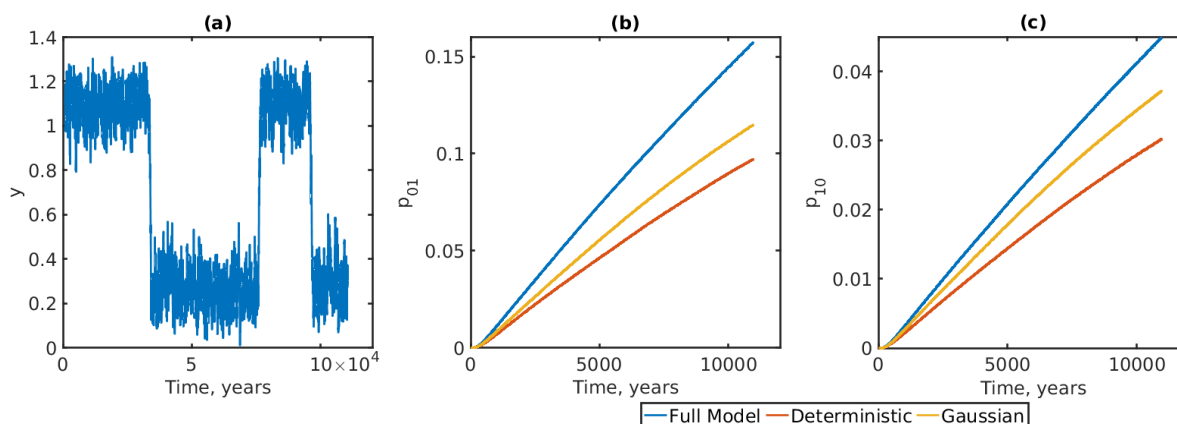497 point, so its distribution converged within the first 504 time units.

Figure 4.   Regime transitions for the three models without mean diffusion. (a) A single $y(t)$ trajectory from the full system showing jumps between regimes. (b) The probability $p_{01}(\tau)$ of a transition from $y(t) < 0.5$ to $y(t + \tau) > 0.8$. (c) The probability $p_{10}(\tau)$ of a transition from $y(t) > 0.8$ to $y(t + \tau) < 0.5$.

498   The climatological distributions of the slow variables are shown in Fig. 3. Panel (a) shows
499 the marginal y distributions of the three models, while panels (b)–(d) show the joint (x, y)
500 distributions. The three models are remarkably similar. Though is the same as in the previ-
501 ous case, P is smaller. The diffusion correction in the x equation of the Gaussian-stochastic
502 approximation has amplitude $\sqrt{5} P^2 x \approx 0.026$ which is smaller than the atmospheric noise
503 amplitude $\sigma_x / \sqrt{\tau} = 0.1$; the atmospheric noise similarly dominates the y equation. As a
504 result, the effects of eddy noise are not seen in the equilibrium distributions of the three models.
505
506   The noise levels are low enough that the system trajectories make rare transitions between
507 the neighborhoods of the two stable equilibria. Fig. 4 panel (a) shows a system trajectory y
508 from the full model that jumps between regimes. The rates and paths of these transitions are
509 the subject of large deviation theory (Freidlin and Wentzell 2012). The methods of Bouchet
510 *et al.* (2016) to analyze the transitions do not seem to apply directly here because of the
511 inclusion of noise forcing in the slow dynamics. In any case, it is not difficult to estimate the
512 transition probabilities from simulations. For practical purposes it was convenient to estimate
513 the following probabilities: $p_{01}(\tau) = P(y(t + \tau) > 0.8 \mid y(t) < 0.5)$ and $p_{10}(\tau) = P(y(t + \tau) <$
514 $0.5 \mid y(t) > 0.8)$. These transition probabilities are plotted for the three models in Fig. 4
515 panels (b) and (c), respectively. The effects of differences in the eddy noise are clear: the
516 deterministic model has the lowest transition probabilities; the Gaussian stochastic model has
517 higher transition probabilities; the full model has the highest transition probabilities.

7.   Conclusions

519 This paper formulates a stochastic two-box ocean model modeled after Stommel's (1961); the
520 model consists of a system of 5 SDEs (1). Previous stochastic Stommel models (e.g. Cessi
521 1994, Vélez-Belchí *et al.* 2001, Monahan *et al.* 2002, Monahan 2002, Monahan and Culina
522 2011), modeled the atmospheric heat and freshwater forcing as Gaussian stochastic processes,
523 and the exchange of heat and salt between the boxes as a nonlinear drift term corresponding
524 to the large-scale overturning thermohaline circulation. The novelty of the formulation here
525 is that a fast, eddy-driven component is added to the the exchange between the boxes. The
526 terms modeling the eddy-driven exchange are quadratic products of approximately Gaussian
527 random variables; products of jointly-Gaussian random fields were recently found to be an
528 accurate model of eddy-driven exchanges in Grooms (2016).
529   In more complete and complex ocean models, fast eddy effects are frequently modeled

530 deterministically. Stochastic parameterizations have recently been developed that multiply
531 these deterministic eddy parameterizations by Gaussian random fields (Andrejczuk *et al.* 2016,
532 Juricke *et al.* 2017), which is a popular approach for atmospheric models based on the work
533 of Buizza *et al.* (1999) and Sura *et al.* (2005). A key benefit of stochastic parameterizations
534 in comparison to deterministic ones is the former's ability to induce realistic variability in the
535 resolved scales. Models with realistic variability are needed for making forecasts with robust
536 uncertainty estimates, which explains the wide adoption of stochastic parameterizations in
537 weather forecasting (Buizza *et al.* 1999, Bell *et al.* 2001, Palmer *et al.* 2005, Berner *et al.*
538 2017, Leutbecher *et al.* 2017).
539   Using methods of averaging and homogenization for slow-fast systems (Pavliotis and Stuart
540 2008, Freidlin and Wentzell 2012, Bouchet *et al.* 2016), two models were derived approximating
541 the evolution of the slow components (the difference in heat and salt content of the two boxes).
542 The first model (5) replaces the fast eddy-driven exchange terms by a fixed 'deterministic' drift
543 term, analogous to the standard approach of deterministic parameterization in more complex
544 ocean models. The second model (7) adds an additional multiplicative noise term accounting
545 for fast variations in the eddy-driven flux. A suite of simulations of each of the three models
546 was used to compare their qualitative behavior in a parameter regime with a single stable
547 equilibrium. All three models were then altered by removing an explicit representation of
548 diffusion and allowing all diffusive effects to be achieved completely by the eddies. Numerical
549 simulations of these models were used to compare their qualitative behavior in a parameter
550 regime with two stable equilibria.
551   The main results are as follows. There is little qualitative difference in the core of the
552 stationary distributions of the full, non-Gaussian model and the Gaussian multiplicative ap-
553 proximation. In the regime with a single equilibrium the deterministic model has too little
554 variability, but the Gaussian model gives an accurate climatological mean and covariance.
555 In the regime with two stable equilibria the climatological distribution of the three models
556 is nearly the same. In the regime with two stable equilibria the amplitude of the eddies is
557 smaller than in the regime with a single equilibrium, which could perhaps account for the fact
558 that the deterministic model is more accurate in the former regime. Observational estimates
559 suggest that up to 30% of the variability of the Atlantic Meridional Overturning Circulation
560 (AMOC) is driven by ocean eddies, with the rest driven by atmospheric noise (Hirschi *et al.*
561 2013, Sonnewald *et al.* 2013).
562   Though the Gaussian stochastic model gives a good approximation of the core of the cli-
563 matological distribution, the rare event probabilities are inaccurate. In the single-equilibrium
564 regime there is no clear trend in the behavior: the Gaussian model overestimates rare event
565 probabilities on one side of the mean, and underestimates on the other side. This inaccuracy
566 manifests for short times, transient behavior too: even with a short lead time, the Gaussian
567 model gives inaccurate predictions of the probability of a rare event. Surprisingly, despite
568 overestimating the climatological rare event probability for one kind of event, in a rare event
569 forecasting configuration the Gaussian model systematically underestimates the rare event
570 probability for both kinds of events (i.e. events above and below the climatological mean).
571   In the regime with two stable equilibria the rare events of interest are the transitions between
572 the two. Despite the fact that the amplitude of the eddy noise in this regime is smaller than the
573 amplitude of the atmospheric noise, clear differences were observed in the rates of transition
574 from the neighborhood of one equilibrium to another: the deterministic model had the rarest
575 transitions, and the Gaussian model still made transitions less frequently than the full model.
576   In the single-equilibrium regime, significant differences in the rare-event dynamics of the
577 three models were only found in the *x* variable, which describes the temperature difference
578 between the poleward and equatorial boxes. The amplitude of the eddy noise in the salinity
579 equation was an order of magnitude smaller than the amplitude of the atmospheric noise, and
580 the latter dominated despite the long-tailed non-Gaussian statistics of the noise in the full

model. In contrast, the amplitude of the eddy noise in the temperature equation was closer to the amplitude of the atmospheric noise, and the effects of non-Gaussianity in the noise were evident in the rare-event statistics. In the regime with two stable equilibria the rare events are transitions between neighborhoods of the two equilibria, and they are most prominent in the salinity rather than the temperature. The amplitude of the eddy noise in this regime is smaller than the amplitude of the atmospheric noise by a factor of about 6, but the long-tailed non-Gaussianity of the eddy noise is still able to have an impact on the rare event probability.

The goal of the investigation was to investigate the qualitative impacts of non-Gaussian eddy noise of the type observed by Grooms (2016) in a simple model, and to compare to models with Gaussian noise and without eddy noise. The extreme simplicity of the model precludes confident extrapolation to more complex and comprehensive ocean models. Nevertheless, the results suggest that Gaussian stochastic parameterizations in ocean general circulation models may be able to successfully produce the day-to-day variability associated with the core of the climatological distribution, but that more accurate non-Gaussian models may be needed to correctly model rare events. Such rare events include extreme behavior like droughts and heat waves, as well as abrupt transitions between climate regimes. The impact of stochastic parameterizations on rare event distributions in climate models has only recently begun to be investigated (Tagle *et al.* 2016).

The qualitative impact of non-Gaussian eddy noise seems to depend on the relative amplitude of that noise in comparison with atmospheric noise forcing. If the eddy noise is significantly smaller than the atmospheric noise, then it will presumably have little impact on the variability of the system. The parameters used here (2) to describe the amplitude of atmospheric and eddy noise are drawn from the literature, but are necessarily imprecise. Hirschi *et al.* (2013) and Sonnewald *et al.* (2013) argue on the basis of observations that up to 30% of the variability of the Atlantic Meridional Overturning Circulation (AMOC) is driven by ocean eddies, with the rest driven by atmospheric noise. Our results suggest that there should be qualitative differences between the rare event probabilities of systems with Gaussian and non-Gaussian eddy models even for noise as small as 30%.

References

Andrejczuk, M., Cooper, F., Juricke, S., Palmer, T., Weisheimer, A. and Zanna, L., Oceanic stochastic parameterizations in a seasonal forecast system. *Mon. Weather Rev.*, 2016, **144**, 1867–1875.

Berner, J., Achatz, U., Batt, L., Bengtsson, L., de la Cmara, A., Christensen, H.M., Colangeli, M., Coleman, D.R.B., Crommelin, D., Dolaptchiev, S.I., Franzke, C.L.E., Friederichs, P., Imkeller, P., Jrvinen, H., Juricke, S., Kitsios, V., Lott, F., Lucarini, V., Mahajan, S., Palmer, T.N., Penland, C., Sakradzija, M., von Storch, J.S., Weisheimer, A., Weniger, M., Williams, P.D. and Yano, J.I., Stochastic Parameterization: Toward a New View of Weather and Climate Models. *Bull. Amer. Meteorol. Soc.*, 2017, **98**, 565–588.

Bouchet, F., Grafke, T., Tangarife, T. and Vanden-Eijnden, E., Large deviations in fast–slow systems. *J. Stat. Phys.*, 2016, **162**, 793–812.

Brankart, J.M., Candille, G., Garnier, F., Calone, C., Melet, A., Bouttier, P.A., Brasseur, P. and Verron, J., A generic approach to explicit simulation of uncertainty in the NEMO ocean model. *Geosci. Model Dev.*, 2015, **8**, 1285.

Buizza, R., Miller, M. and Palmer, T., Stochastic Simlulation of Model Uncertainties in the ECMWF Ensemble Prediction System. *QJR Meteorol. Soc*, 1999, **125**, 28887–2908.

Cessi, P., A simple box model of stochastically forced thermohaline flow. *J. Phys. Ocean.*, 1994, **24**, 1911–1920.

629 Cooper, F.C., Optimisation of an idealised primitive equation ocean model using stochastic parameterization.
630   *Ocean Model.*, 2017, **113**, 187–200.
631 Cotter, C.J., Gottwald, G.A. and Holm, D.D., Stochastic partial differential fluid equations as a diffusive limit
632   of deterministic Lagrangian multi-time dynamics. *P. R. Soc. A*, 2017, **473**.
633 Deshayes, J., Tr´eguier, A.M., Barnier, B., Lecointre, A., Sommer, J.L., Molines, J.M., Penduff, T., Bourdall´e-
634   Badie, R., Drillet, Y., Garric, G. *et al.*, Oceanic hindcast simulations at high resolution suggest that the
635   Atlantic MOC is bistable. *Geo. Res. Lett.*, 2013, **40**, 3069–3073.
636 Freidlin, M. and Wentzell, A., *Random perturbations of dynamical systems*, Third revised and enlarged edition
637   edn, 2012 (Springer).
638 Grooms, I., A Gaussian-product stochastic Gent–McWilliams parameterization. *Ocean Modelling*, 2016, **106**,
639   27–43.
640 Grooms, I., Lee, Y. and Majda, A.J., Numerical schemes for stochastic backscatter in the inverse cascade of
641   quasigeostrophic turbulence. *Multiscale Model. Sim.*, 2015, **13**, 1001–1021.
642 Held, I.M., The gap between simulation and understanding in climate modeling. *B. Am. Meteorol. Soc.*, 2005,
643   **86**, 1609–1614.
644 Higham, D.J., Mao, X. and Stuart, A.M., Strong convergence of Euler-type methods for nonlinear stochastic
645   differential equations. *SIAM J. Numerical Analysis*, 2002, **40**, 1041–1063.
646 Hirschi, J., Blaker, A., Sinha, B., Coward, A., de Cuevas, B., Alderson, S. and Madec, G., Chaotic variability
647   of the meridional overturning circulation on subannual to interannual timescales. *Ocean Science*, 2013, **9**,
648   805–823.
649 Holm, D.D., Variational principles for stochastic fluid dynamics. *P. R. Soc. A*, 2015, **471**, 20140963.
650 Hutzenthaler, M., Jentzen, A. and Kloeden, P.E., Strong and weak divergence in finite time of Euler's method
651   for stochastic differential equations with non-globally Lipschitz continuous coefficients. *Proc. R. Soc. Lond.*
652   *Ser. A Math. Phys. Eng. Sci.*, 2011, **467**, 1563–1576.
653 Juricke, S., Palmer, T.N. and Zanna, L., Stochastic Subgrid-Scale Ocean Mixing: Impacts on Low-Frequency
654   Variability. *J. Climate*, 2017, **30**, 4997–5019.
655 Khasminskii, R., *Stochastic stability of differential equations*, Second edition edn, 2012 (Springer).
656 Kloeden, P.E. and Platen, E., *Numerical solution of Stochastic Differential Equations*, 1992 (Springer).
657 Lamba, H., Mattingly, J.C. and Stuart, A.M., An adaptive Euler–Maruyama scheme for SDEs: Convergence
658   and stability. *IMA journal of numerical analysis*, 2007, **27**, 479–506.
659 Leutbecher, M., Lock, S.J., Ollinaho, P., Lang, S.T., Balsamo, G., Bechtold, P., Bonavita, M., Christensen,
660   H.M., Diamantakis, M., Dutra, E., English, S., Fisher, M., Forbes, R.M., Goddard, J., Haiden, T., Hogan,
661   R.J., Juricke, S., Lawrence, H., MacLeod, D., Magnusson, L., Malardel, S., Massart, S., Sandu, I., Smo-
662   larkiewicz, P.K., Subramanian, A., Vitart, F., Wedi, N. and Weisheimer, A., Stochastic representations of
663   model uncertainties at ECMWF: State of the art and future vision. *QJR Meteorol. Soc*, 2017.
664 Mao, X. and Szpruch, L., Strong convergence and stability of implicit numerical methods for stochastic differ-
665   ential equations with non-globally Lipschitz continuous coefficients. *Journal of Computational and Applied*
666   *Mathematics*, 2013, **238**, 14–28.
667 Mattingly, J.C., Stuart, A.M. and Higham, D.J., Ergodicity for SDEs and approximations: locally Lipschitz
668   vector fields and degenerate noise. *Stochastic processes and their applications*, 2002, **101**, 185–232.
669 M´emin, E., Fluid flow dynamics under location uncertainty. *Geophysical & Astrophysical Fluid Dynamics*, 2014,
670   **108**, 119–146.
671 Monahan, A.H., Alexander, J. and Weaver, A.J., Stochastic models of the meridional overturning circula-
672   tion: time scales and patterns of variability. *Philosophical Transactions of the Royal Society of London A:*
673   *Mathematical, Physical and Engineering Sciences*, 2008, **366**, 2525–2542.
674 Monahan, A.H. and Culina, J., Stochastic averaging of idealized climate models. *J. Climate*, 2011, **24**, 3068–
675   3088.
676 Monahan, A.H., Correlation effects in a simple stochastic model of the thermohaline circulation. *Stochastics*
677   *and Dynamics*, 2002, **2**, 437–462.
678 Monahan, A.H., Timmermann, A. and Lohmann, G., Comments on Noise-induced transitions in a simplified
679   model of the thermohaline circulation. *J. Phys. Ocean.*, 2002, **32**, 1112–1116.
680 Orrell, D., Smith, L., Barkmeijer, J. and Palmer, T., Model error in weather forecasting. *Nonlinear Proc.*
681   *Geoph.*, 2001, **8**, 357–371.
682 Palmer, T., Shutts, G., Hagedorn, R., Doblas-Reyes, F., Jung, T. and Leutbecher, M., Representing model
683   uncertainty in weather and climate prediction. *Annu. Rev. Earth Planet. Sci.*, 2005, **33**, 163–193.
684 Papanicolaou, G. and Kohler, W., Asymptotic theory of mixing stochastic ordinary differential equations.
685   *Communications on Pure and Applied Mathematics*, 1974, **27**, 641–668.
686 Pavliotis, G. and Stuart, A., *Multiscale Methods Averaging and Homogenization*, 2008 (Springer).
687 Porta Mana, P. and Zanna, L., Toward a stochastic parameterization of ocean mesoscale eddies. *Ocean Model.*,
688   2014, **79**, 1–20.
689 Rahmstorf, S., Bifurcations of the Atlantic thermohaline circulation in response to changes in the hydrological
690   cycle. *Nature*, 1995, **378**, 145.
691 Resseguier, V., M´emin, E. and Chapron, B., Geophysical flows under location uncertainty, Part I Random
692   transport and general models. *Geophys. Astro. Fluid*, 2017, **111**, 149–176.
693 Schmitt, R.W., Salinity and the Global Water Cycle. *Oceanography*, 2008, **21**, 12.
694 Sonnewald, M., Hirschi, J.J.M., Marsh, R., McDonagh, E.L. and King, B.A., Atlantic meridional ocean heat

transport at 26N: impact on subtropical ocean heat content variability. *Ocean Science*, 2013, **9**, 1057–1069.

Stammer, D., Global characteristics of ocean variability estimated from regional TOPEX/POSEIDON altimeter measurements. *J. Phys. Ocean.*, 1997, **27**, 1743–1769.

Stommel, H., Thermohaline convection with two stable regimes of flow. *Tellus*, 1961, **13**, 224–230.

Sura, P., Newman, M., Penland, C. and Sardeshmukh, P., Multiplicative noise and non-Gaussianity: A paradigm for atmospheric regimes?. *J. Atmos. Sci.*, 2005, **62**, 1391–1409.

Tagle, F., Berner, J., Grigoriu, M.D., Mahowald, N.M. and Samorodnitsky, G., Temperature Extremes in the Community Atmosphere Model with Stochastic Parameterizations. *J. Climate*, 2016, **29**, 241–258.

V´elez-Belch´ı, P., Alvarez, A., Colet, P., Tintor´e, J. and Haney, R., Stochastic resonance in the thermohaline circulation. *Geo. Res. Lett.*, 2001, **28**, 2053–2056.

Williams, P.D., Howe, N.J., Gregory, J.M., Smith, R.S. and Joshi, M.M., Improved Climate Simulations through a Stochastic Parameterization of Ocean Eddies. *J. Climate*, 2016, **29**, 8763–8781.

Zanna, L., Mana, P.P., Anstey, J., David, T. and Bolton, T., Scale-aware deterministic and stochastic parametrizations of eddy-mean flow interaction. *Ocean Model.*, 2017, **111**, 66–80.